RELATIONSHIP BETWEEN SOLAR WIND ELECTRIC FIELD AND GEOMAGNETIC ACTIVITY IN INCREASING AND DECREASING PHASES OF SOLAR WIND VELOCITY

Tadanori ONDOH

Space Earth Environment Laboratory, Kitano, Tokorozawa 359-1152

Abstract: Solar wind velocity normally increases to a maximum above 600 km/s from a quiet value below 400 km/s in a few days and returns to the quiet one in a week. We select 445 time profiles of solar wind velocity data with simple variation in the interval from January 1964 to April 1985. Averaged ΣK_p values at the solar wind velocity of 500 km/s are 28 and 19 in the increasing (leading) and decreasing (trailing) phases of solar wind velocity for the above time-profiles, respectively. The maximum ΣK_p was found to occur around the middle in the leading phase, to statistically coincide with a large southward IMF-Bz ($\leqq -4$ nT) with duration longer than 5 hours. The K_p rapidly increased with increasing the southward IMF in first 10 hours of the geomagnetic storm on July 22–25,1974. A maximum $K_p = 7$ occurred together with a maximum westward solar wind electric field (VBz) of -6.9 mV/m. Correlative variations of AE with VBz continued from 22 UT, July 22 to 11 UT, July 23 when a maximum southward IMF-Bz of -12.4 nT occurred. After 11 UT, July 23, the correlation between VBz and AE became irregular. It is concluded that, for the initial storm phase, the solar wind electric field directly penetrates into the polar magnetosphere along interconnected field lines and produces higher AE indices. After the maximum southward IMF, the magnetic merging could no longer occur at the dayside magnetopause. Rapid AE increases associated with Dst decreases are discussed in terms of the ring current and the cross-tail current. The AE activities after the maximum southward IMF seem to be related with magnetospheric processes which are independent of the solar wind electric field.

1. Introduction

The solar wind energy drives magnetospheric substorms and geomagnetic storms. Since SNYDER *et al.* (1963) demonstrated a correlation of $V = 8.44 \Sigma K_p + 330$ km/s between the daily sum of geomagnetic activity indices (ΣK_p) and solar wind velocity V, a number of studies have shown correlations of the solar wind velocity and IMF-Bz with geomagnetic activity indices (ONDOH and HAKURA, 1964; MURAYAMA and HAKAMADA, 1975; BAKER *et al.*, 1981; HOLZER and SLAVIN, 1982). The importance of IMF-Bz in the solar wind-magnetosphere coupling was also noted by many researchers (FAIRFIELD and CAHILL, 1966; ARNOLDY, 1971; FOSTER *et al.*, 1971; MENG *et al.*, 1973). The combined interplanetary parameter VBz has been used as an index of the solar wind-magnetosphere coupling (AUBRY and McPHERRON, 1971; ROSTOKER *et al.*, 1972; HOLZER and SLAVIN, 1978; MELONI *et al.*, 1982; MAEZAWA and MURAYAMA, 1986). The time constant for the magnetospheric response to the solar wind changes has been estimated to be 20–60 min by using superposed epoch analysis, cross-correlation analy-

sis and measurements of time delays (FOSTER *et al.*, 1971; CAAN *et al.*, 1978; BAKER *et al.*, 1981). Studies on the energy coupling between the solar wind and magnetosphere was reviewed by AKASOFU (1981). However, these authors conducted the correlation studies only for geomagnetic disturbances lasting below a few days. In the vicinity of Earth's orbit, the solar wind velocity occasionally increases from a quiet value below 400 km/s to above 600 km/s within a few days, and then it decreases from the maximum to the quiet value for a week.

In this paper, we compare time variations of the solar wind parameters with those of ΣK_p for 445 time profiles of solar wind velocity with monotonic rise and fall variations selected from the Interplanetary Medium Data book (KING, 1977, 1979; COUZENS and KING, 1986). Firstly, we show a statistical coincidence of ΣK_p maximum with large and long southward IMF-Bz on time scales of about 10 days. Secondly, we compare time variations of the solar wind electric field VBz and the solar wind dynamic pressure with those of K_p and AE indices for a geomagnetic storm of July 22–25, 1974. These results are discussed in terms of the dayside magnetic merging of the southward IMF and northward geomagnetic field in the dayside outer magnetosphere.

2. Difference of ΣK_p Dependence on Solar Wind Velocity between Solar Wind Leading and Trailing Phases

The momentum of high-speed solar plasma stream exerts a large pressure on the plasma at the solar wind leading edge, causing the plasma pressure, density, and magnetic field to build up and form a compression region (WHANG, 1991). This region is called an interaction region (BURLAGA and OGILVIE, 1970; BURLAGA, 1984). The interaction region is observed as clearly defined increases in pressure, magnetic field strength, and the general level of fluctuation around 1 AU. The upper panel of Fig. 1 shows a time variation of solar wind velocity and ΣK_p values from July 22 to 29, 1974 are indicated at the bottom of the panel. The lower panel of Fig. 1 shows IMF-B and -Bz (nT) for the same period. In the solar wind leading phase, the solar wind velocity, V_s, increased rapidly from 350 km/s to above 750 km/s within one day of July 23. In an interaction period (22 UT, July 22–11 UT, July 23), the IMF-B enhanced rapidly above 20 nT, and the IMF-Bz decreased simultaneously below -9 nT with a duration of about 10 hours. In this period, the southward IMF seems to have reconnected with the northward geomagnetic field in the dayside magnetosphere, and caused a dayside magnetic merging. The ΣK_p increased rapidly from 14 on July 22 ($V_s = 330$ km/s) to a maximum of 47 on July 23 ($V_s = 500$ km/s). Then, the ΣK_p decreased slowly from the maximum to 21 on July 29 ($V_s = 500$ km/s) in the solar wind trailing phase. Between July 24 and 30, the IMF-B remained around 5 nT and IMF-Bz varied within ± 3 nT. As shown by downward arrows in Fig. 1, $\Sigma K_p = 47$ in the solar wind leading phase is greater than $\Sigma K_p = 21$ in the trailing phase at $V_s = 500$ km/s.

Using 445 monotonic rise and fall variations in the solar wind velocity selected from the Interplanetary Medium Data books (KING, 1977, 1979; COUZENS and KING, 1986), we obtained two statistical distributions of ΣK_p at $V_s = 500$ km/s in the leading and trailing phases from 445 time profiles of solar wind velocity as shown in Fig. 2. The ΣK_p average of 28 and standard deviation of 7.8 for the leading phase are clear-
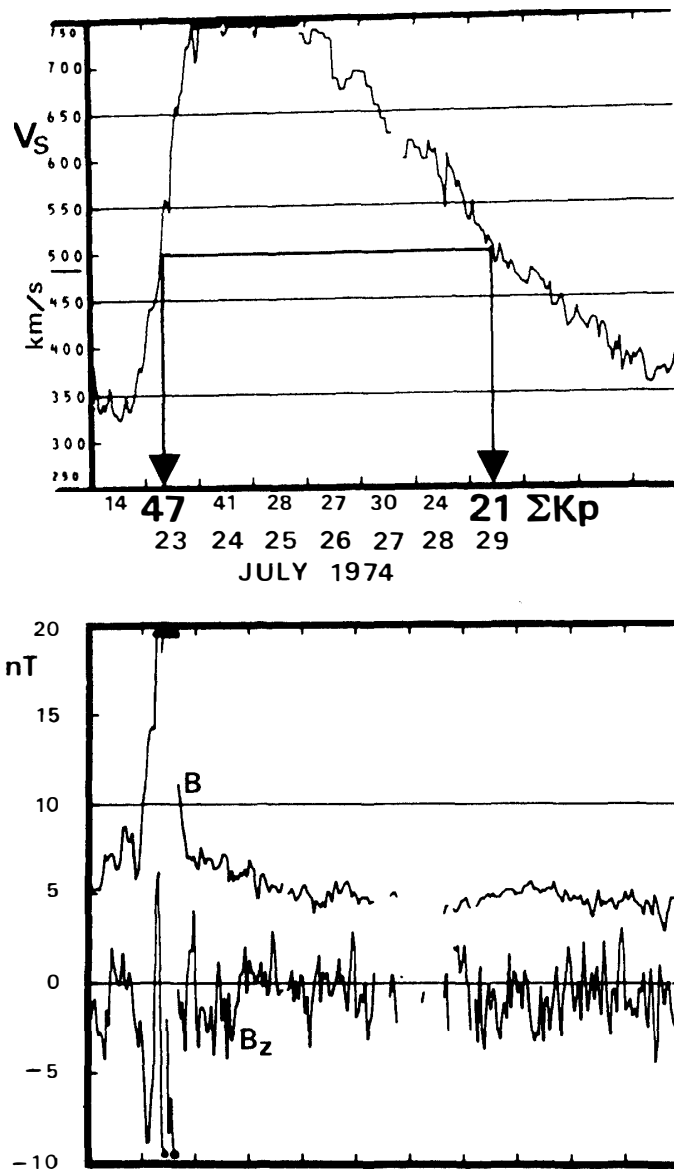
Fig. 1.   *Time variations in solar wind bulk velocity, Vs, and ΣK_p (bottom numerals) in an upper panel, and in IMF-B and IMF-Bz (GSM coordinate) in a lower panel between July 22 and 30, 1974. Downward arrows indicate $\Sigma K_p = 47$ in the increasing phase of solar wind velocity and $\Sigma K_p = 21$ in the decreasing phase of solar wind velocity at $V_s = 500$ km/s.*

ly larger than 19 and 7.1 for the trailing phase. The maximum ΣK_p in the trailing phase overlaps the lower half of the high ΣK_p values in the leading phase. A main reason of this result is due to the occurrence of maximum ΣK_p around the midway in the solar wind leading phase.
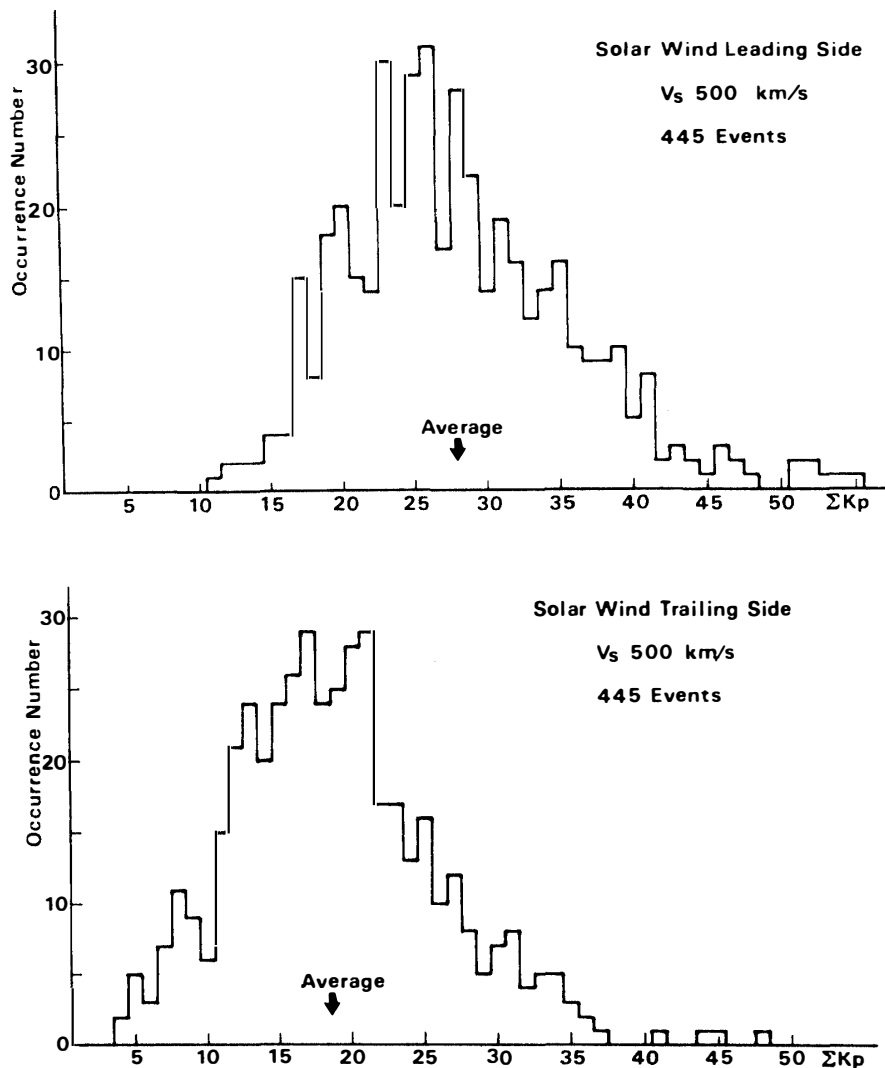
Fig. 2. Occurrence distributions of ΣK_p at the solar wind velocity of 500 km/s in the solar wind leading phase (upper panel), and in the solar wind trailing phase (lower panel) obtained from 445 time profiles of solar wind velocity with monotonic rise and fall variations from January, 1964 to April, 1985.

3. Coincidence of Maximum ΣK_p with Maximum Southward IMF

When the interaction region with the southward IMF arrives at the dayside magnetopause, the dayside magnetic merging occurs in the dayside outermost magnetosphere (DUNGEY, 1961). A solid line and solid circles in the upper panel of Fig. 3 show time variations of the solar wind velocity and ΣK_p from May 4 to 11, 1971, respectively. The solar wind velocity increased from 400 km/s before May 5 to a maximum of 680 km/s on May 7, while ΣK_p increased rapidly from 14 on May 5 to a maximum of 39 on May 6. Thus, the maximum ΣK_p occurs normally around the mid-

way in the solar wind leading phase. The lower panel of Fig. 3 shows time variations of the total IMF intensity B and IMF-Bz. A maximum IMF of $B = 13$ nT and a maximum southward IMF of $Bz = -9$ nT occurred together with a maximum ΣK_p of 39 on May 6. In the trailing phase, the ΣK_p returned already to rather quiet value of 22 on May 8, when the solar wind velocity was still above 600 km/s. This results from the K_p definition that a slow recovery of geomagnetic field decrease in the long recovery phase is not taken into account of the K_p or K scalings, and also from the maximum ΣK_p occurrence around the midway in the increasing phase of solar wind velocity.
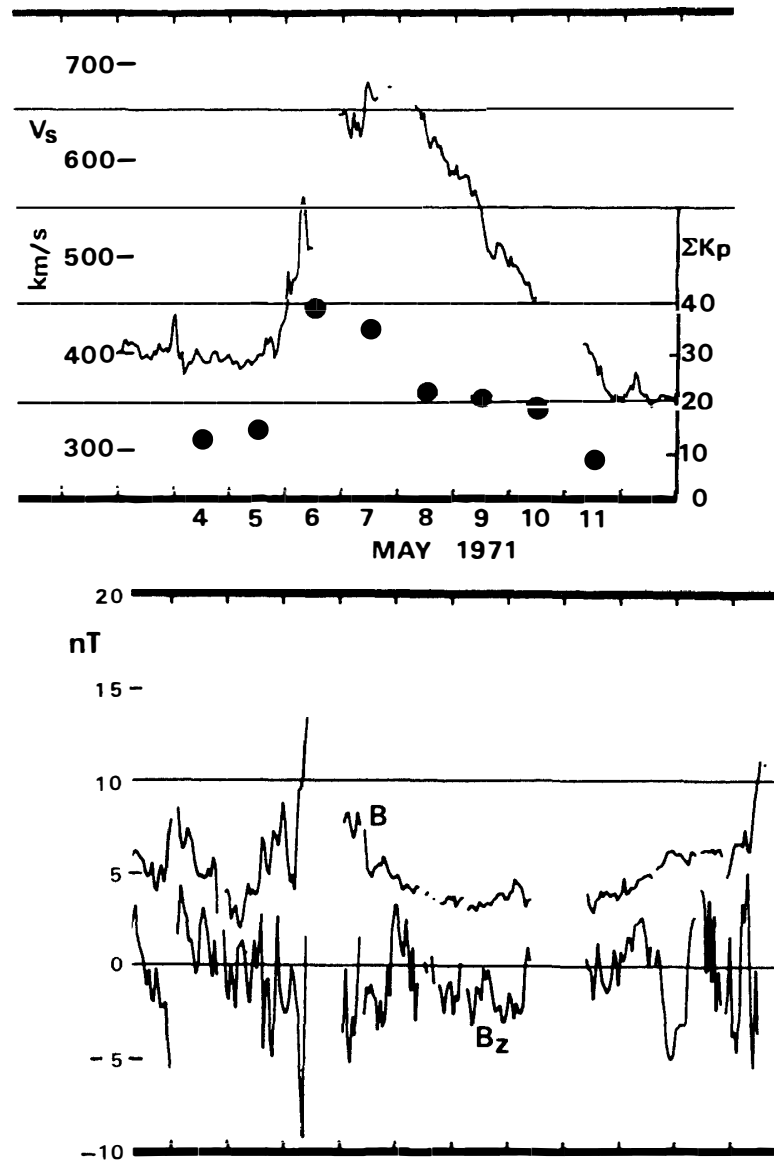

Fig. 3.   Time variations in solar wind bulk velocity, V, and ΣK_p (solid circles) in an upper panel, and those in IMF-B and IMF-Bz (GSM coordinate) in a lower panel from May 4 to May 11, 1974.

Next, we study this relationship with more data. The IMF-Bz observations are available for 152 of the selected 445 time profiles of solar wind velocity data. Of these, we further selected 117 time profiles of the solar wind velocity in which the maximum ΣK_p coincided with the maximum southward IMF-Bz in order to obtain the occurrence rate of the southward IMF-Bz intensity, southward IMF-Bz duration, and coincident maximum ΣK_p.

The coincident occurrence rate of the maximum ΣK_p with the maximum southward IMF-Bz is 0.77 ($=117/152$). In the remaining cases, the maximum ΣK_p did not
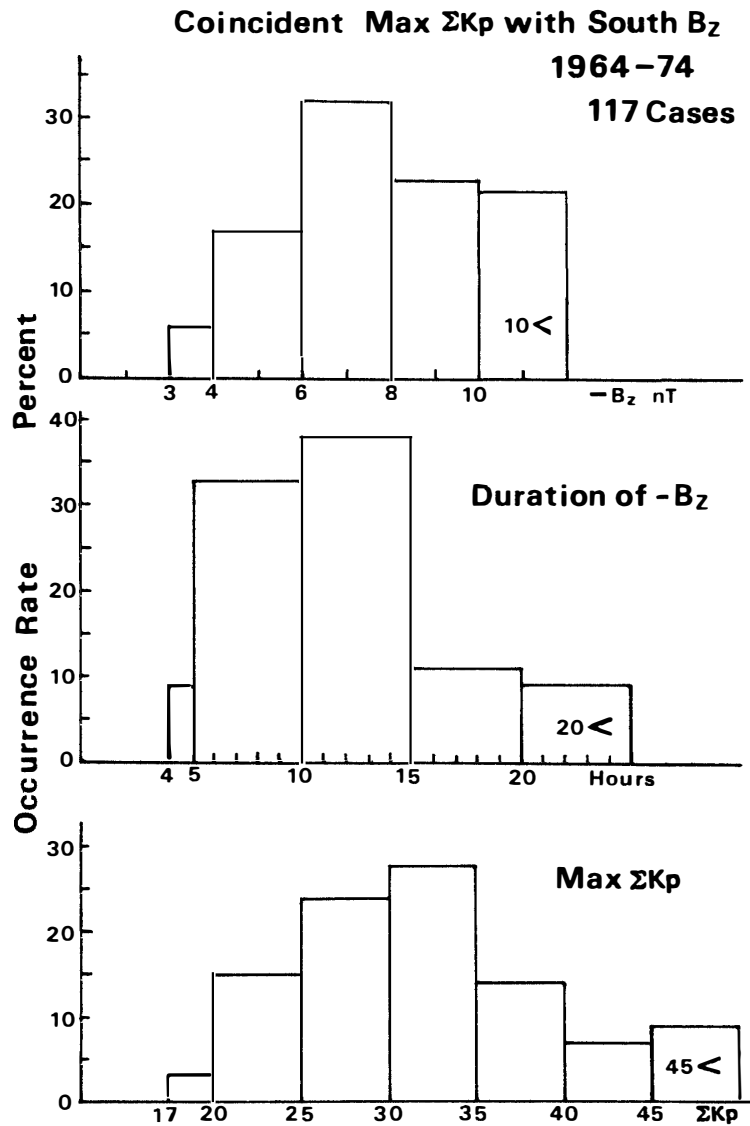

Fig. 4. Occurrence rate distributions of southward IMF-Bz intensity (nT) in upper panel, southward IMF-Bz duration (hour) in middle panel, and the corresponding maximum ΣK_p in 117 cases when a southward IMF-Bz occurred coincidently with a maximum ΣK_p on the leading phase of solar wind velocity in bottom panel.

correspond to a large ($Bz \leqq -4$ nT) and long ($\geqq 5$ hours) southward IMF-Bz. Such ΣK_p maxima may be caused by successive strong substorms, but not by a single geomagnetic storm, since a substorm lasts for about one hour. Figure 4 shows, from top to bottom, three distributions of the occurrence rate for the southward IMF-Bz intensity, southward IMF-Bz duration and coincident maximum ΣK_p obtained from 117 profiles of the solar wind velocity. We notice in the diagrams that a maximum $\Sigma K_p (\geqq 20)$ occurred on the same day when a large southward IMF-Bz from -4 nT to -20 nT continued for a long time above 5 hours. As a statistical aspect, the maximum ΣK_p is clearly related to large and long-lasting southward IMF-Bz in the solar wind leading phase.

4. Comparison of Time Variations of Solar Wind Electric Field and K_p for a Geomagnetic Storm of July 22–25, 1974

The solar wind electric field, VBz has been discussed as an index of solar wind-magnetosphere coupling where V is the solar wind velocity and Bz is the Z- component (N-S) of interplanetary magnetic field in the GSM coordinate (Aubry and McPherron, 1971; Rostoker et al., 1972; Holzer and Slavin, 1978; Meloni et al., 1982; Maezawa and Murayama, 1986). The solar wind has many irregularities on different time and spatial scales depending upon their evolution and their relative propagation velocity. Simultaneous observations of the solar wind by the Interball and Wind satellites show remarkably different time profiles of solar wind velocity, magnetic field, and plasma density on time scales below 30 minutes outside the Earth's magnetosphere. Approximately same time profiles of solar wind velocity were observed on time scales above several tens of minutes by the two satellites which were separated by a distance over 10 Earth's radii (Nemecek et al., 1996). Consequently, we use hourly values of solar wind data in order to avoid undesirable effects of the solar wind irregularities on the following data analysis. We discuss effects of the solar wind electric field and IMF-Bz on the geomagnetic activity by comparing time variations of VBz and IMF-Bz with those of K_p and AE observed from July 22 to August 2, 1974. In this period, a large geomagnetic storm during which K_p attained to 7 occurred for July 22–25, 1974 as shown by Figs. 5a–c. We used three hourly averages of V or Bz as defined by $V(0-3) = (V_0 + V_1 + V_2 + V_3)/4$, where V_i is an hourly value at the i-th hour, for comparing VBz with three hourly indices of K_p.

Figures 5a–c show three kinds of histograms; the upper one is VBz (mV/m), the middle one is K_p, and the bottom one is the solar wind dynamic pressure P_s (dyne/cm^2), where 1 mV/m $= 1000$ nT·km/s (1 nT $= 10^{-9}$ Wb/m^2 and 1 Wb $= 1$ Vs). The monthly quiet days were July 22, 30, 31, and August 1, 1974. The monthly disturbed days were July 23 and 24. The solar wind velocity became maximum (826 km/s) just before the midnight of July 24 when the geomagnetic storm had already been recovering. Negative values of VBz represent westward electric fields for southward IMF's. The solar wind electric fields can enter into the polar magnetosphere along southward interplanetary magnetic field lines connected to northward geomagnetic field lines by the dayside magnetic merging. So, good correlations of K_p with VBz may be caused by direct penetration of the westward solar wind electric fields into the polar magneto-

sphere along interconnected field lines. For 12–18 UT, July 22, there were northward IMF-Bz, eastward VBz for K_p below 2. For 21–00 UT, July 22, a geomagnetic storm of $K_p=3$ occurred as a southward IMF and westward VBz of -2.4 mV/m appeared. For 00–03 UT, July 23, the geomagnetic storm developed up to $K_p=5$ for a southward IMF-$Bz=-5$ nT and $VBz=-2.7$ mV/m. For 03–06 UT, July 23, the geomagnetic storm further developed ($K_p=6$) for IMF-$Bz=-7$ nT and $VBz=-3.2$ mV/m. For 06–09 UT, July 23, a northward IMF of $Bz=1$ nT and an eastward electric field of $VBz=0.5$ mV/m appeared, but K_p remained at 5. Since K_p is determined by geomagnetic data observed at subauroral zone stations, it represents global geomagnetic activity mainly caused by the auroral electrojet, equatorial ring current, and mid-latitude ionospheric current. In an initial storm period when the ring current has not yet developed well, correlations between K_p and VBz seem to indicate the dayside magnetic merging effect. Since the southward IMF, westward VBz, and K_p increased monotonically with time from 21–00 UT, July 22 to 03–06 UT, July 23, the dayside merging region seems to have come deeper into the dayside magnetosphere as stronger southward interplanetary magnetic fields subsequently arrived at the outer magnetosphere. Northward IMF's for 06–09 UT, July 23 ($Bz=4.4$ nT at 07 UT and 6.2 nT at 08 UT) could not recover well developed disturbances and K_p was $5-$. In this case,

(a)
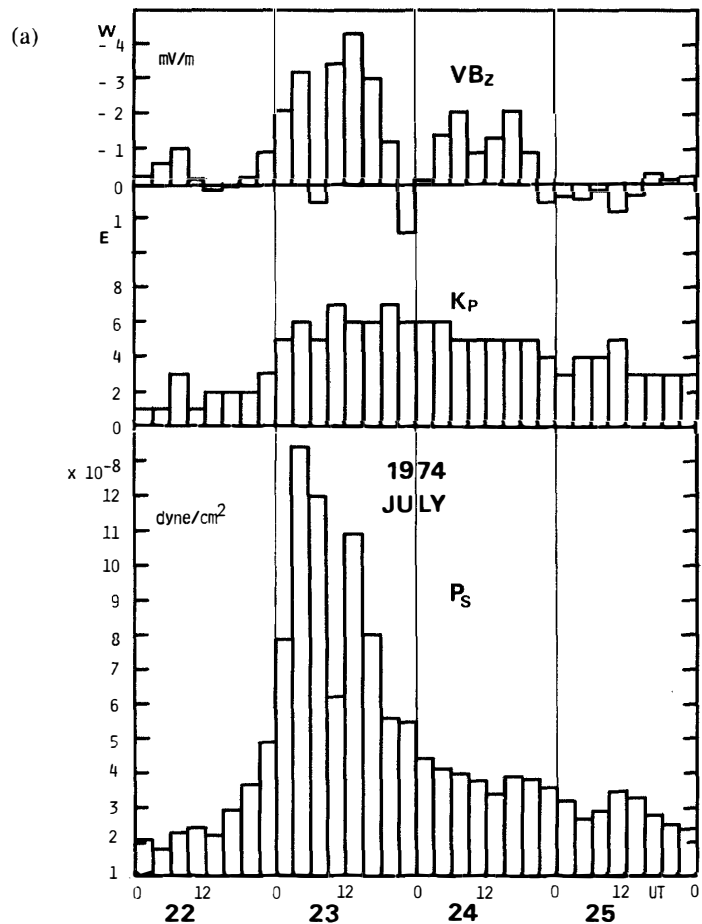
Figs. 5a–c. Time variations for three hourly averages of solar wind electric field VBz (mV/m), where the upward direction is the westward electric field in upper section, those for K_p in middle section, and those for three hourly averages of solar wind dynamic pressure($\times 10^{-8}$ dyne/cm²) in bottom section from July 22 to July 25 (a), from July 26 to July 29 (b), and from July 30 to August 2, 1974 (c).
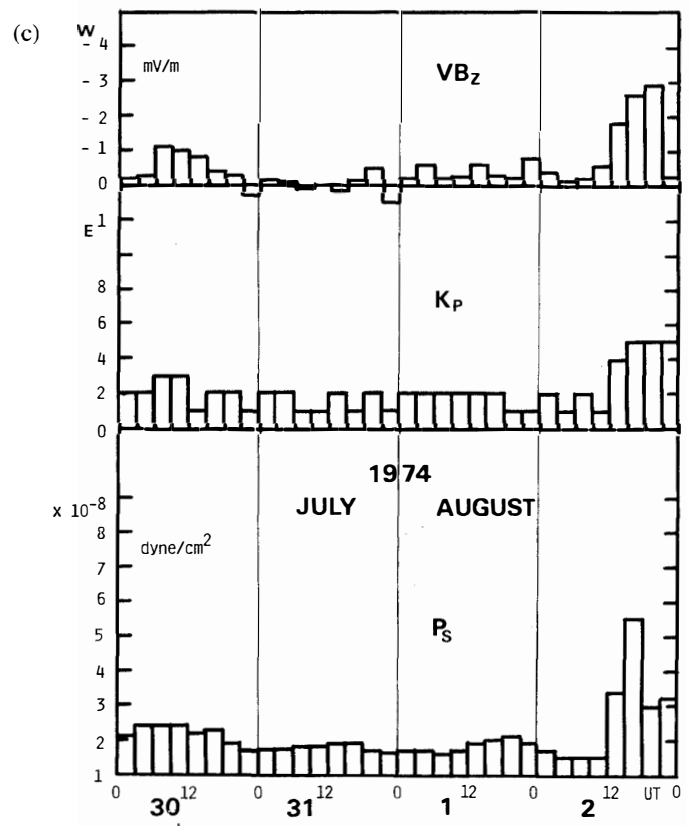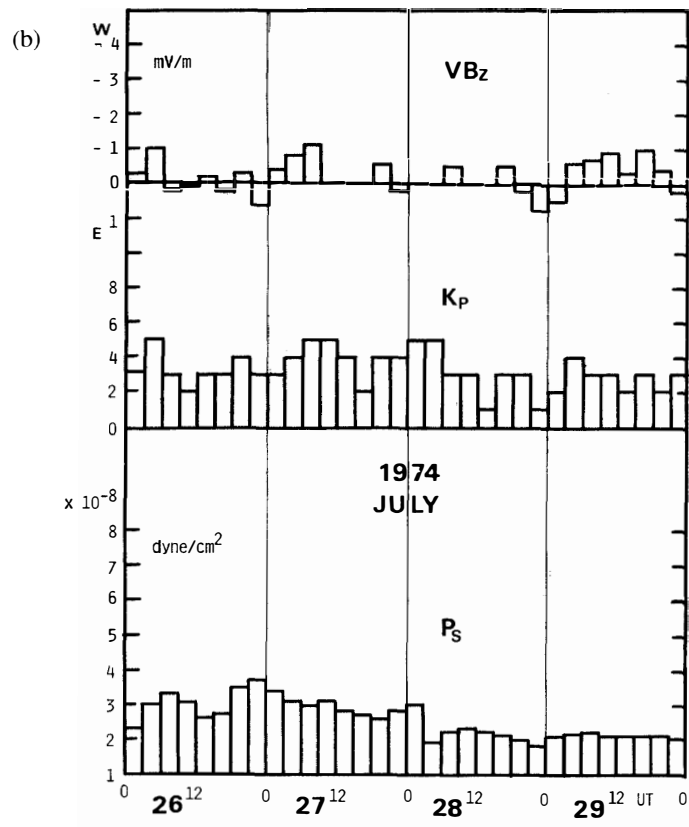
(b)

(c)

Fig. 5   (Continued).

the northward IMF seems to have reconnected with southward geomagnetic fields on higher latitude sides of the north and south cusps, and to have added newly formed closed geomagnetic field lines onto the dayside magnetosphere. So, open tailward stretched field lines caused by previous dayside mergings would be separated from the Earth and would be carried away by the solar wind. Then, southward IMF's of $Bz = -9.1$ nT at 10 UT and -12.4 nT at 11 UT above those before 06 UT, July 23 again caused the dayside magnetic mergings, and produced a maximum $K_p = 7$ and westward electric field of $VBz = -6.1$ mV/m for 09–12 UT, July 23. For 12–15 UT, southward IMF's of $Bz = -1.9$ nT (12 UT), -8.3 nT (13 UT), -6.4 nT (14 UT) and -10.8 nT (15 UT) caused $VBz = -4.3$ mV/m and $K_p = 6_+$. However, for 18–21 UT, July 23, weak southward IMF's of $Bz = -2.0$ nT (18 UT), -1.0 nT (19 UT), -3.7 nT (20 UT), and 0.0 nT (21 UT) correspond to $VBz = -1.2$ mV/m and $K_p = 7_-$. Since the northward turning of the IMF-Bz at the maximum solar wind velocity of 826 km/s for 21–00 UT, July 24, high K_p's between 6_- and 5 occurred between 21 UT, July 23 and 21 UT, July 24 for IMF-Bz's within ± 3 nT and solar wind velocities above 700 km/s. These high geomagnetic activities were not related to the southward IMF and westward VBz, and so the K_p's after 12 UT, July 23 seem to be caused by magneto-spheric processes, such as particle precipitations and field-aligned currents associated with the equatorial ring currents or magnetospheric convection through the viscous-like momentum transfer from the solar wind to the magnetosphere (AXFORD and HINES, 1961). Thus, the dayside magnetic merging proceeds deeper into the magnetosphere as larger southward IMF subsequently arrives at the dayside magnetosphere. But, after the arrival of maximum southward IMF, the northward geomagnetic field in the dayside outermost magnetosphere becomes larger than newly arriving southward IMF, and the dayside merging can no longer occur in the outer magnetosphere.

The day of July 31 is the most quiet day of four monthly quiet days of July 22, 30, 31, and August 1, 1974 in solar and geomagnetic activity conditions. As shown by Fig. 5c, southward IMF's with $Bz > -3$ nT for VBz within ± 1 mV/m often occurred even on the monthly quiet days. In other words, the northward IMF is not always sufficient and essential conditions for a geomagnetic quiet day.

5. Rapid Increase of Solar Wind Dynamic Pressure in Initial Storm Period

The solar wind dynamic pressure, $P_s = nmV^2$ was 4.9×10^{-8} dyne/cm^2 for 21–00 UT ($K_p = 3$), July 22 when the IMF-Bz turned southward, and was 7.9×10^{-8} dyne/cm^2 for 00–03 UT ($K_p = 5_-$), July 23 (Fig. 5a), where n is the proton density (cm^{-3}), m the proton mass, and V the solar wind velocity.

The dynamic pressure attained to a maximum of 13.4×10^{-8} dyne/cm^2 for 03–06 UT ($K_p = 6$), July 23, and then decreased down to 12.0×10^{-8} dyne/cm^2 for 06–09 UT ($K_p = 5_-$), July 23 when the IMF-Bz temporarily turned northward. Thus, the solar wind dynamic pressure increased rapidly, and compressed the dayside magnetosphere to cause the dayside magnetic merging in initial ten hours after a storm beginning, though this storm had no sc. For 09–12 UT, July 23, the dynamic pressure significantly decreased to 6.2×10^{-8} dyne/cm^2 and caused a maximum $K_p = 7$ for $VBz = -3.4$ mV/m. For 12–15 UT, it again increased to 10.9×10^{-8} dyne/cm^2 and caused

$K_p = 6_+$ for a maximum $VBz = -4.3$ mV/m. For 18–21 UT, July 23, the dynamic pressure considerably decreased to 5.6×10^{-8} dyne/cm^2 and a high geomagnetic activity of $K_p = 7_-$ occurred for $VBz = -1.2$ mV/m. After 21 UT, July 23, the solar wind dynamic pressure decreased slowly with time, and it varied below 4×10^{-8} dyne/cm^2 until August 2, 1974.

As to time variations of the solar wind dynamic pressure and VBz, the solar wind plasma seems to consist of two interaction regions with the southward IMF for 00–06 UT, July 23 and for 09–18 UT, July 23 which were separated by a northward IMF period of 06–09 UT, July 23.

6. Correlative Time Variations of AE with VBz for a Geomagnetic Storm of July 22–25, 1974

Figures 6a–c show time variations of hourly values for solar wind velocity, V (thin line), solar wind dynamo electric field, VBz (thick line), storm-time geomagnetic horizontal field variation, Dst (thin line), and auroral electrojet index, AE (thick line) from July 22 to 27, 1974. Negative VBz values of westward solar wind electric field are plotted in the upward direction of ordinate in Figs. 6a–c. The Dst curve in Fig. 6a shows an initial storm increase around 15 UT, July 22 and a storm Dst decrease caused by an equatorial ring current began around 22 UT, July 22, together with a southward IMF turning (-2.4 nT) and an increase of westward solar wind electric field. Overall variations of VBz and AE are similar to each other in Fig. 6a.
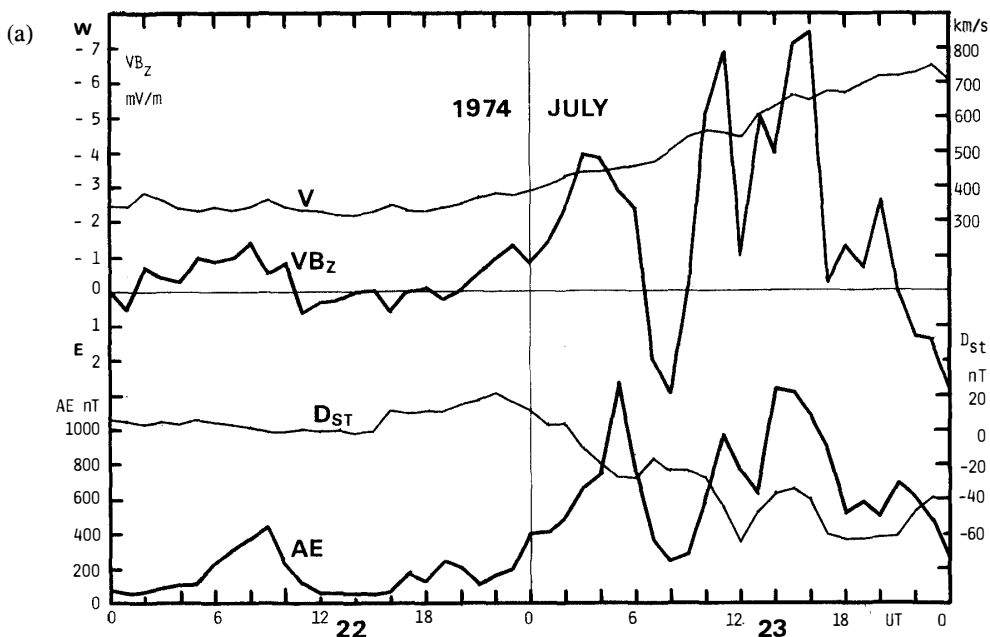
Figs. 6a–c. Time variations for hourly values of solar wind velocity, V (upper thin line, km/s), solar wind electric field, VBz (upper thick line, the westward field being upward in mV/m), Dst (lower thin line, nT), and AE (lower thick line, nT) from July 22 to July 23 (a), from July 24 to July 25 (b), and from July 26 to July 27, 1974 (c).
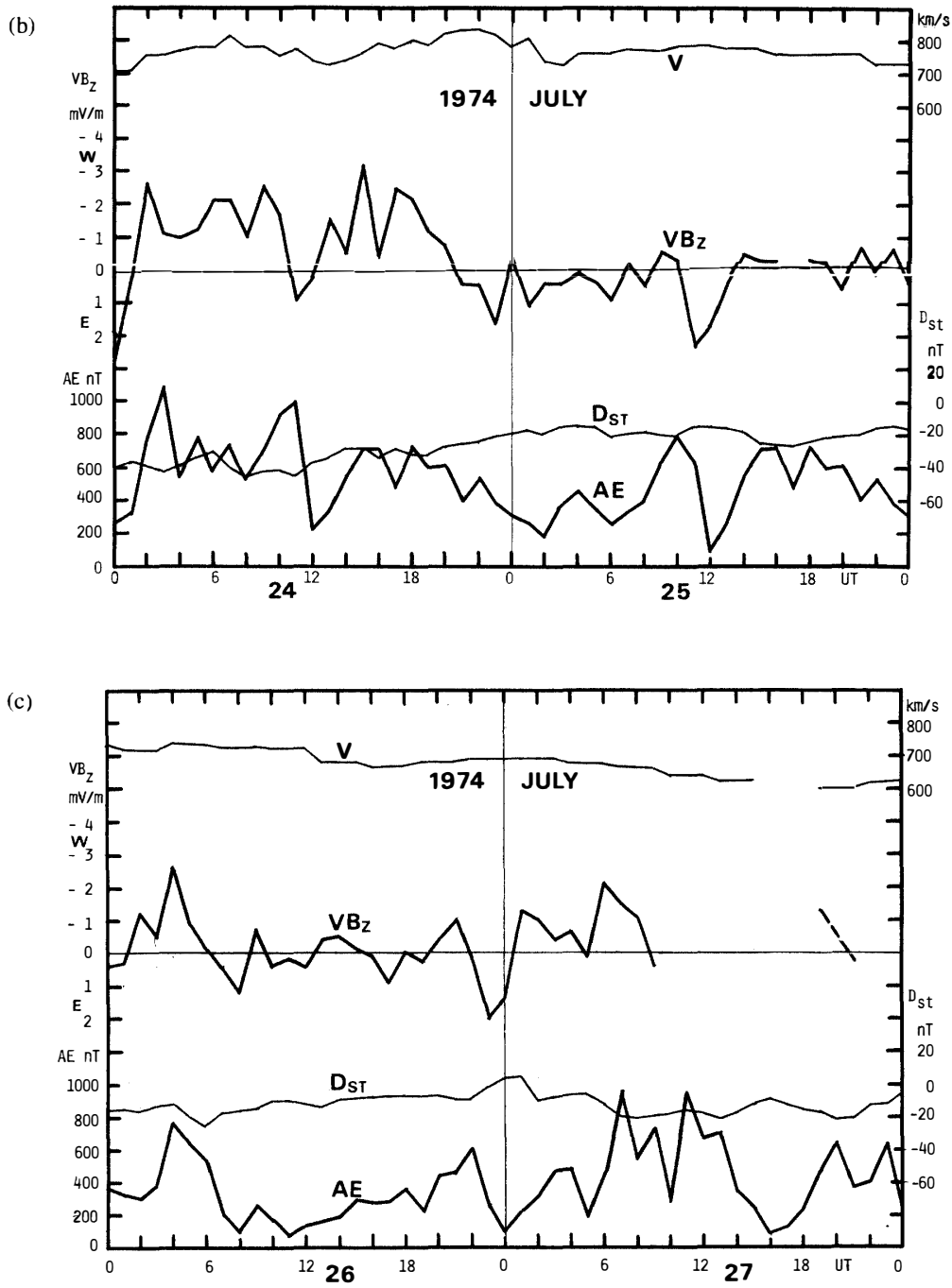
Fig. 6 (Continued).

Plasmasheet particles drift inward as an westward electric field increases. Accelerated ions drift westwards and accelerated electrons drift eastwards around the Earth inside the plsamasheet inner edge (ONDOH and AIKYO, 1987). They produce the ring current (WILLIAMS, 1983). As discussed in the solar wind dynamic pressure, high *AE* activities above 500 nT occurred in the two groups in 00–06 UT and in 09–18 UT, July 23 for large westward electric fields.

The *Dst* curve indicates that the geomagnetic storm, *i.e.* equatorial ring current developed between 06 UT and 22 UT, July 23. We discuss in detail a relationship between *AE* and *VBz* in the latter group. Detailed time variations of *VBz* and *AE* corresponded well to each other from 22 UT, July 22 to 11 UT, July 23 when the maximum southward IMF of $Bz = -12.4$ nT occurred. Akasofu (1980) has indicated that the solar wind dynamo operates even when the solar-magnetosphere energy coupling is weak or is in a quiet condition. So, the *AE* activities between 22 UT, July 22 and 11 UT, July 23 were produced by penetration of the westward solar wind electric fields into the polar magnetosphere along the interconnected field-lines caused by the dayside merging, except for a northward IMF period of 07–09 UT, July 23. Northward IMF's of $Bz = 4.4$ nT at 07 UT and 6.2 nT at 08 UT, July 23 corresponded well to *AE* decreases between 06 and 10 UT, July 23. From 12 UT to 14 UT, July 23, there was no peak to peak correlation between *AE* and *VBz* for southward IMF's of $Bz = -1.9$ nT (12 UT), -8.3 nT (13 UT) and -6.4 nT (14 UT) and for a $VBz = -4.3$ mV/m (12–15 UT). Then, large *AE* increases at 15 and 16 UT, July 23 occurred for large southward IMF's of $Bz = -10.8$ nT (15 UT) and -11.4 nT (16 UT) and for $VBz = -4.0$ mV/m.

In 18–21 UT, July 23, large $K_p = 7_-$ occurred for a large *Dst* decrease, while small *AE*'s below 400 nT occurred for small southward IMF's of $Bz = -3$ nT (17 UT), -2.0 nT (18 UT), and -1.0 nT (19 UT). Between 11 UT of the maximum southward IMF and 18 UT, July 23, the *AE* time variation lagged or advanced about one hour behind or before the *VBz*(or IMF-*Bz*) time variation. Such time differences between the *VBz* and *AE* variations may be caused by magnetospheric processes, such as ionization enhancements due to particle precipitation, or by cessation of the dayside magnetic merging.

At 00 UT, July 24, a northward IMF of $Bz = 4.1$ nT (eastward $VBz = 2.9$ mV/m) occurred together with $P_s = 4.5 \times 10^{-8}$ dyne/cm^2, and time variations of *VBz* and *AE* simultaneously became minimum as shown in Figs. 6a and b. Figures 6b and c show that the time variation of *AE* lagged one hour behind that of *VBz* from 18 UT, July 23 to 18 UT, July 24 except for 00 UT, July 24. After 18 UT, July 24, the time variation of AE lagged more than one hour behind that of *VBz*, and the correspondence between the both variations became irregular as shown in Figs. 6b and c.

In summary, after the maximum southward IMF of $Bz = -12.4$ nT at 11 UT, July 23, the solar wind electric field seems not to have penetrated into the polar magnetosphere along the interconnected field lines since the dayside magnetic merging can occur only when a stronger IMF newly arrives at the dayside magnetosphere. Although the correlative time variations of AE for 13–16 UT, July 23 apparently correspond to large westward *VBz* and southward IMF-*Bz* between -6.4 nT and -11.4 nT, the *AE* activities after the maximum southward IMF at 11 UT, July 23 seem to be caused by the magnetospheric process, such as particle precipitations and field-aligned currents associated with the equatorial ring current (*Dst* decrease), an inward movement of the plasmasheet inner edge and the Alfvén layer phenomena which are independent of the solar wind electric field.

7.   Discussions on Magnetospheric Processes for AE Increases Associated with Dst Decreases

As shown in Fig. 6a, the westward solar wind electric field (negative VBz) and the AE index began to increase together with the Dst decrease after 22 UT, July 22 and also large AE increases occurred during large storm-time Dst decreases. This suggests the following magnetospheric process. An westward solar wind electric field which penetrates into the magnetosphere causes a sunward drift of plasmasheet ions and electrons. When they reach a region of dipolar geomagnetic field, the ions and electrons, respectively, drift westward and eastward around the Earth to produce an equatorial ring current (Dst decrease).

In a steady state collisionless plasma in the magnetic field, the force due to the plasma.pressure gradient, $-\nabla P$, which confines the particles, must be balanced by the Lorentz force $\mathbf{I} \times \mathbf{B}$. This is given by $\nabla \mathbf{P} = \mathbf{I} \times \mathbf{B}$ where $\mu_0 \mathbf{I} = \nabla \times \mathbf{B}$ and μ_0 is the magnetic permeability in the vacuum. As for the equatorial ring current of hot plasma, an outward Lorentz force due to an eastward current and the northward geomagnetic field balances an inward pressure force, $-\nabla \mathbf{P}$ inside the plasma pressure peak, since the particle distributions in the ring current have the pressure peak around $L = 3\sim4$. Also, an inward Lorentz force due to a westward current and the geomagnetic field balances an outward pressure force outside the plasma pressure peak.

The total ring current, $\mathbf{I}$ due to the particle distribution is given by

$$\mathbf{I} = (\mathbf{B}/B^2) \times [\nabla P_\perp + (P_\parallel - P_\perp)\,(\mathbf{B} \cdot \nabla)\,\mathbf{B}/B^2],$$

where $\mathbf{P}_\perp$ and $\mathbf{P}_\parallel$ are the particle pressures normal and parallel to the geomagnetic field, $\mathbf{B}$, respectively (PARKER, 1957). The magnetic field perturbation ΔB ($\simeq Dst$) at the Earth's center due to the ring current is given by

$$\Delta B/B_0 = -2E_R/3E_M,$$

where B_0 is the geomagnetic field at the earth's surface, E_R is the total kinetic energy of the ring current particles and E_M is the total energy of the Earth's dipole field above the Earth's surface (DESSLER and PARKER, 1959). The total ring current dominated by the pressure gradient term consists of an eastward current inside the pressure peak ($L\sim3$) in the ring current, and an extended westward current ($L = 3\sim8$) due to the pressure gradient at geocentric distances outside the pressure peak around $L\sim3$ in the ring current (WILLIAMS, 1987).

The magnetospheric substorm may be produced by the magnetic reconnection in the near-Earth tail caused by enhancements of antiparallel open geomagnetic fluxes in the magnetospheric lobe region. As the westward solar wind electric field intensifies the inward plasma drift in the plasmasheet, the inner edge of the cross tail current sheet approaches to the dipolar geomagnetic field region.

When the inward drifting particles enter into the dipolar field region, the ring current begins to flow around the Earth by the geomagnetic field gradient drift of plasma particles. Then, the eastward current, which is opposite to the westward cross-tail current, locally flows in an inner-front region of the ring current inside a plasma pressure peak formed by a pressure pile-up of the inward plasma against the dipolar field

region. This situation is favorable for the cross-tail current disruption associated with the magnetic reconnection which occurs in the near-Earth tail at a very rapid AE increase or substorm onset.

As the ring current develops, a northward diamagnetic field of the ring current on the far side of the ring current may weaken a southward diamagnetic field of the cross-tail current near the inner edge of the cross-tail current sheet. This is also favorable for a subsequent magnetic reconnection associated with an inward movement of the cross-tail current sheet in a period of large Dst decreases, such as the AE increases for 09–17 UT, July 23. Thus, the ring current seems to provide favorable conditions for generating the rapid AE increase or substorm.

Next, we discuss the energy conversion between the electromagnetic and kinetic energies in the solar wind-magnetosphere interaction (HEIKKILA, 1978; ATKINSON, 1980; HILL, 1983). The energy flow in the magnetosphere is given by the Poynting flux relation neglecting the dielectric current;

$$\nabla(\mathbf{E} \times \mathbf{H}) + \mu_0 \, \partial H^2 / 2 \partial t = -\mathbf{E} \cdot \mathbf{J}.$$

The first term and the second term on the left hand side are the electromagnetic Poynting flux, and the time derivative of magnetic energy density, respectively. The right hand side is the conversion rate of electromagnetic energy to kinetic energy. As for the magnetospheric problem, the time derivative of magnetic energy density may represent the time variation of magnetic energy density stored in the magnetosphere. In the above equation, the local conversion rate of magnetic energy to kinetic energy, $\mathbf{E} \cdot \mathbf{J}$ is equivalent to the local convergence of electromagnetic energy flow plus the stored magnetic energy density.

When an westward solar wind electric field, $\mathbf{E} = -\mathbf{V} \times \mathbf{B}$ is generated in a southward IMF of $\mathbf{B}$, $\mathbf{E} \cdot \mathbf{J} > 0$ for westward currents, $\mathbf{J}$ on the dayside magnetopause between the northern and southern cusps and for westward equatorial cross-tail currents. While $\mathbf{E} \cdot \mathbf{J} < 0$, when eastward magnetopause currents flow on the polar side of the both cusps in the southward IMF. In the southward IMF, the plasma acceleration or particle heating may occur on the dayside magnetopause between the both cusps and in the tail plasma sheet since the magnetic energy is transferred into the kinetic energy for $\mathbf{E} \cdot \mathbf{J} > 0$. In other words, the Ohm's law, $\mathbf{E} = \eta \mathbf{J} - \mathbf{V} \times \mathbf{B}$ gives an expression of $\mathbf{E} \cdot \mathbf{J} = \eta J^2 + \mathbf{V}(\mathbf{J} \times \mathbf{B})$ where $\eta = 1 / \sigma$ is the electric resistivity. The first and second terms on the right-hand side of the above equation represent the Joule heating and the plasma acceleration due to the Lorentz force, respectively. While open geomagnetic fluxes caused by the dayside merging are added to latitudes higher than the cusp from the dayside magnetosphere since the kinetic energy is transferred into the magnetic energy for $\mathbf{E} \cdot \mathbf{J} < 0$.

On the other hand, when an eastward solar wind electric field occurs in a northward IMF, $\mathbf{E} \cdot \mathbf{J} < 0$ for the westward dayside magnetopause currents between the both cusps and for the westward equatorial cross-tail currents, and $\mathbf{E} \cdot \mathbf{J} > 0$ for the eastward magnetopause currents flowing at latitudes above the both cusps. Consequently, closed geomagnetic fluxes caused by the cusp reconnection in the northward IMF are newly added to the outer dayside magnetosphere between the both cusps since the kinetic energy is transferred into the magnetic energy for $\mathbf{E} \cdot \mathbf{J} < 0$. Also, for the westward tail

currents, the particle energy spectrum in the plasmasheet becomes softer, and the plasmasheet inner edge recedes tailward because of $\mathbf{E} \cdot \mathbf{J} < 0$. While the tailward stretching open geomagnetic field lines previously caused by the dayside merging are separated from the Earth by the cusp reconnection on the polar side of both cusps since the magnetic energy is transferred into the kinetic energy by $\mathbf{E} \cdot \mathbf{J} > 0$. This produces a geomagnetic flux decrease in the magnetotail. Thus, the AE decreases between 07 and 09 UT, July 23 are explained by a cusp latitude increase, by a closed geomagnetic flux increase on the dayside magnetopause between the both cusps caused by the cusp reconnection between the southward open geomagnetic field lines and northward IMF on the polar side of the both cusps, and also by the tailward recession of the plasmasheet inner edge.

8. Conclusion

The solar wind velocity increases rapidly from 350 km/s to a maximum above 600 km/s within a few days and decreases to 350 km/s within a week near the Earth. The maximum ΣK_p occurs around the middle in the increasing phase of solar wind velocity. Two average values of ΣK_p at solar wind velocity of 500 km/s in the increasing (leading) and decreasing (trailing) phases of solar wind velocity are statistically obtained from 445 time profiles of the solar wind velocity with monotonic rise and fall variation. The average value and standard deviation of ΣK_p for the two phases are 28 and 7.8 in the leading phase, and 19 and 7.1 in the trailing phase, respectively. From 117 time profiles of solar wind velocity in which a maximum ΣK_p coincides with a maximum southward IMF-Bz, it is statistically found that the maximum ΣK_p coincides with a large southward IMF-Bz below -4 nT lasting above 5 hours.

Time variations of solar wind parameters were also compared with those of K_p and AE for a geomagnetic storm of July 22–25 ,1974. The geomagnetic storm without sc began just after a southward IMF turning for 21–00 UT, July 22, 1974.

This storm had two periods of high solar wind dynamic pressure above 7×10^{-8} dyne/cm^2 for 00–09 UT and 12–18 UT, July 23, 1974. The increases of the solar wind dynamic pressure compressed the dayside magnetosphere and the large southward IMF's subsequently caused the dayside magnetic mergings in the initial storm phase of about 10 hours. The K_p increased with increasing westward solar wind electric field from 21 UT, July 22 to 06 UT, July 23. The maximum southward IMF of $Bz = -12.4$ nT at 11 UT after $Bz = -9.1$ nT at 10 UT, July 23 produced a maximum $K_p = 7$ for 09–12 UT, July 23 in the storm main phase of $Dst = -60$ nT.

Time variations of the AE correlated well with those of the solar wind electric field for 21 UT, July 22 to 11 UT, July 23 even in the period of northward IMF for 07–09 UT, July 23. This suggests that the westward solar wind electric field penetrated into the polar magnetosphere along interconnected field lines caused by the dayside magnetic merging in the southward IMF period, and produced higher AE activities. The ring current seems to provide favorable conditions for generating a rapid AE increase or substorm in the near-Earth tail region.

In the northward IMF period, the cusp magnetic merging may occur between the northward IMF and southward open tailward stretching fields on the polar side of the

cusp magnetopause, of which latitude increased together with a tailward recession of the plasmasheet inner edge.

Time variations of *AE* indices did not correlate well with those of solar wind electric fields VBz after the maximum southward IMF at 11 UT, July 23. The *AE* activities after the maximum southward IMF may be produced by magnetospheric processes independent of the solar wind electric field.

References

AKASOFU, S.-I. (1980): What is a magnetospheric substorm? Dynamics of the Magnetosphere, ed. by S.-I. AKASOFU. Dordrecht, D. Reidel, 447–460.

AKASOFU, S.-I. (1981): Energy coupling between the solar wind and the magnetosphere. Space Sci. Rev., **28**, 121–190.

ATKINSON, G. (1980): The expansive phase of the magnetospheric substorm. Dynamics of the Magnetosphere, ed. by S.-I. Akasofu. Dordrecht, D. Reidel, 461–481.

ARNOLDY, R. L. (1971): Signature in the interplanetary medium for substorms. J. Geophys. Res., **76**, 5189–5201.

AUBRY, M. P. and McPHERRON, R. L. (1971): Magnetotail changes in relation to the solar wind magnetic field and magnetospheric substorms. J. Geophys. Res., **76**, 4381–4401.

AXFORD, W.I. and HINES, C. O. (1961): A unifying theory of high latitude geophysical phenomena and geomagnetic storms. Can. J. Phys., **39**, 1433–1464.

BAKER, D. N., HONES, E. W., PAYNE, J. B., Jr. and FELDMAN, W. C.(1981): A high-time resolution study of interplanetary parameter correlation with *AE*. Geophys. Res. Lett., **8**, 179–182.

BURLAGA, L. F. (1984): MHD processes in the outer heliosphere. Space Sci. Rev., **39**, 255–316.

BURLAGA, L. F. and OGILVIE, K. W. (1970): Magnetic and thermal pressures in the solar wind. Solar Phys., **15**, 61–71.

CAAN, M. N., McPHERRON, R. L. and RUSSELL, C. T. (1978): The statistical magnetic signature of magnetospheric substorms. Planet. Space Sci., **26**, 269–279.

COUZENS, D. A. and KING, J. H. (1986): Interplanetary medium data book. NSSDC/WDC-A-R&S, 86–04.

DESSLER, A. J. and PARKER, E. N. (1959): Hydromagnetic theory of geomagnetic storms. J. Geophys. Res., **64**, 2239–2252.

DUNGEY, J. W. (1961): Interplanetary magnetic field and the auroral zones. Phys. Rev. Lett., **6**, 47–48.

FAIRFIELD, D. H. and CAHILL, L. J. (1966): Transition region magnetic field and polar magnetic disturbances. J. Geophys Res., **71**, 155–169.

FOSTER, J. C., FAIRFIELD, D. H., OGILVIE, K. W. and ROSENBERG, T. J. (1971): Relationship of interplanetary parameters and occurrence of magnetospheric substorms. J. Geophys. Res., **76**, 6971–6975.

HEIKKILA, W. J. (1978): Electric field topology near the dayside magnetopause. J. Geophys. Res., **83**, 1071–1078.

HILL, T. W. (1983): Solar-wind magnetosphere coupling. Solar-Terrestrial Physics, ed. by R. L. CAROVILLANO and J. M. FORBES. Dordrecht, D. Reidel, 261–302.

HOLZER, R. E. and SLAVIN, J. A. (1978): Magnetic flux transfer associated with expansions and contractions of the dayside magnetosphere. J. Geophys. Res., **83**, 3831–3839.

HOLZER, R. E. and SLAVIN, J. A. (1982): An evaluation of three predictions of geomagnetic activity. J. Geophys. Res., **87**, 2558–2562.

KING, J. H. (1977): Interplanetary medium data book. NSSDC/WDC-A-R&S 77–04.

KING, J. H. (1979): Interplanetary medium data book. NSSDC/WDC-A-R&S 79–08.

MAEZAWA, K. and MURAYAMA, T. (1986): Solar wind velocity effects on the auroral zone magnetic disturbances. Solar Wind-Magnetosphere Coupling, ed. by Y. KAMIDE and J. A. SLAVIN. Tokyo, Terra Sci. Publ., 59–83.

MELONI, A., WOLF, A. and LANZEROTTI, L. J. (1982): On the relationship between interplanetary quantities and the global auroral electrojet index. J. Geophys. Res., **87**, 119–127.

MENG, C.-I., TSURUTANI, B., KAWASAKI, K. and AKASOFU, S.-I. (1973): Cross-correlation analysis of the

AE index and the interplanetary magnetic field B_z component. J. Geophys. Res., **78**, 617–629.

MURAYAMA, T. and HAKAMADA, K. (1975): Effects of solar wind parameters on the development of magnetospheric substorms. Planet. Space Sci., **23**, 75–91.

NEMECEK, Z., SAFRANKOVA, J., ZASTENKER, G. and TRISKA, P. (1996): Multipoint study of the solar wind: Interball contribution to the topic. Abstracts, 31st Scientific Assembly of COSPAR, The University of Birmingham, 169.

ONDOH, T. and AIKYO, K. (1987): Effects of tailward stretching geomagnetic field on drift motion of plasma particles in the magnetospheric equatorial plane. Adv. Space Res., **6**, 203–208.

ONDOH, T. and HAKURA, Y. (1964): Relation between the solar plasma velocity and the geomagnetic activity. Rep. Ionos. Space Res. Jpn., **18**, 287–290.

PARKER, E. N. (1957): Newtonian development of the dynamical properties of ionized gases at low density. Phys. Rev., **107**, 924.

ROSTOKER, G., LAM, H.-L. and HUME, W. D. (1972): Response time of the magnetosphere to the interplanetary electric field. Can. J. Phys., **50**, 544–547.

SNYDER, C. W., NEUGEBAUER, M. and RAO, U. R. (1963): The solar wind velocity and its correlation with cosmic ray variations and with solar and geomagnetic activity. J. Geophys. Res., **68**, 6361–6370.

WHANG, Y. C. (1991): Shock interactions in the outer heliosphere. Space Sci. Rev., **57**, 339–388.

WILLIAMS, D. J. (1983): The earth's ring current: Causes, generation and decay. Space Sci. Rev., **34**, 223–234.

WILLIAMS, D. J. (1987): The Earth's ring current: Present situation and future thrusts. Phys. Scrip., **T18**, 140–151.